Journal of Contaminant Hydrology 238 (2021) 103773

Contents lists available at ScienceDirect

Journal of Contaminant Hydrology

journal homepage: www.elsevier.com/locate/jconhyd

Combined method of $^{3}H/^{3}He$ apparent age and on-site helium analysis to identify groundwater flow processes and transport of perchloroethylene (PCE) in an urban area

Christian Moeck [a,*], Andrea L. Popp [a,b,1], Matthias S. Brennwald [a], Rolf Kipfer [a,b,c], Mario Schirmer [a,d]

[a] Department of Water Resources and Drinking Water, Eawag, Swiss Federal Institute of Aquatic Science and Technology, Dübendorf, Switzerland
[b] Department of Environmental Systems Science, ETH Zurich, Zurich, Switzerland
[c] Department of Earth Sciences, ETH Zurich, Zurich, Switzerland
[d] Centre of Hydrogeology and Geothermics (CHYN), University of Neuchâtel, Neuchâtel, Switzerland

ARTICLE INFO

Keywords:
Groundwater transport
Managed aquifer recharge (MAR)
3H/3He apparent age
Environmental gases
Perchloroethylene
Aquifer connectivity

ABSTRACT

Urban groundwater management requires a thorough and robust scientific understanding of flow and transport processes. $^{3}H/^{3}He$ apparent ages have been shown to efficiently help provide important groundwater-related information. However, this type of analysis is expensive as well as labor- and time-intensive, and hence limits the number of potential sampling locations.

To overcome this limitation, we established an inter-relationship between $^{3}H/^{3}He$ apparent groundwater ages and ^{4}He concentrations analyzed in the field with a newly developed portable gas equilibrium membrane inlet mass spectrometer (GE-MIMS) system, and demonstrated that the results of the simpler GE-MIMS system are an accurate and reliable alternative to sophisticated laboratory based analyses. The combined use of $^{3}H/^{3}He$ lab-based ages and predicted ages from the $^{3}H/^{3}He$–^{4}He age relationship opens new opportunities for site characterization, and reveals insights into the conceptual understanding of groundwater systems.

For our study site, we combined groundwater ages with hydrochemical data, water isotopes (^{18}O and ^{2}H), and perchloroethylene (PCE) concentrations (1) to identify spatial inter-aquifer mixing between artificially infiltrated groundwater and water originating from regional flow paths and (2) to explain the spatial differences in PCE contamination within the observed groundwater system. Overall, low PCE concentrations and young ages occur when the fraction of artificially infiltrated water is high. The results obtained from the age distribution analysis are strongly supported by the information gained from the isotopic and hydrochemical data. Moreover, for some wells, fault-induced aquifer connectivity is identified as a preferential flow path for the transport of older groundwater, leading to elevated PCE concentrations.

1. Introduction

Increasing population and water demands for industrial, agricultural, and household uses, combined with climate change, is leading to an imbalance of water supply and demand in many regions, and challenging water resource management (e.g. Burri et al., 2019; de Graaf et al., 2014; Gleeson et al., 2012; Minnig et al., 2018). Especially in urban areas with industrial zones, the supply of drinking water from groundwater sources is further complicated due to potential groundwater contamination (Bertrand et al., 2016; Navarro and Carbonell, 2007). Water management in such areas is recognized as a very complex task, both in terms of different spatial and temporal scales (Schirmer et al., 2013; Vázquez-Suñé et al., 2005). Contaminated sites are often the foremost concern for groundwater quality. It is problematic if these sites are located in the vicinity of drinking water production areas, potentially leading to decreased water quality and posing a potential risk to both human health and the environment (Baillieux et al., 2015; Karges et al., 2018).

Thus, sustainable and efficient water management practices within these environments require a thorough scientific understanding of flow

* Corresponding author.
E-mail address: Christian.moeck@eawag.ch (C. Moeck).
[1] Present address: Department of Geoscience, University of Oslo, Norway.

https://doi.org/10.1016/j.jconhyd.2021.103773
Received 6 September 2020; Received in revised form 13 January 2021; Accepted 14 January 2021
Available online 22 January 2021

and transport processes, as well as groundwater residence time (e.g. Chambers et al., 2019; Gooddy et al., 2006; Manning and Caine, 2007; McCallum et al., 2014). Assessing groundwater flow paths and residence times is critical for the exploitation of aquifers, and developing adequate groundwater protection plans in particular. However, adequate quantification of these processes is often challenged by complex geological settings and subsurface heterogeneity (e.g. Cirpka and Kitanidis, 2000; Koltermann and Gorelick, 1996; Moeck et al., 2020; Poeter and Gaylord, 1990; Regli et al., 2003), which cannot be fully explored (Fienen et al., 2009; Kitanidis, 2015; Renard, 2007). As a result, both the spatial distribution of contaminants within an aquifer and the time needed for water quality changes to propagate through the system are not completely understood (Szabo et al., 1996). Strategies to protect drinking water production sites are often based on limited data and thus limited system knowledge (Mackay et al., 1985; Moeck et al., 2016).

Environmental tracers have been shown to efficiently determine the sources and residence times of groundwater, offering insight into the flow and transport behavior of contaminants (Battle-Aguilar et al., 2017; Cook and Böhlke, 2000; McCallum et al., 2014; Schilling et al., 2019). Since the majority of groundwater contamination in urban areas has occurred in recent times (< 100 years), tritium (^{3}H) is a suitable tracer for younger groundwater (up to 60 years in age; e.g. Kipfer et al., 2002). Tritium was released between the late 1950s and early 1960s in high amounts, mainly into the stratosphere, by thermonuclear bomb tests (Cook and Herczeg, 2012; Massmann et al., 2009). In combination with its decay product, helium (^{3}He), tritium provides an age measure independent of the tritium input (Cook and Solomon, 1997). This makes it advantageous as a tracer, as it eliminates the necessity to establish the exact time-dependent tritium delivery to the aquifer. Helium produced by ^{3}H decay accumulates in groundwater and does not undergo any chemical reactions, making it an ideal tracer. There exist different sources of ^{3}He that define the total ^{3}He (^{3}He$_{tot}$). These are the concentration in solubility equilibrium with the atmosphere (^{3}He$_{eq}$), the component originating from excess air (^{3}He$_{ex}$), terrigenic components derived from the crust and mantle (^{3}He$_{ter}$), and the source that comes from the decay of tritium (^{3}He$_{tri}$) (see Kipfer et al., 2002 for a review). The different components can be estimated and fractions can be subsequently subtracted from ^{3}He$_{tot}$ thanks to the complementary measurements of other noble gases (more details can be found in Kipfer et al., 2002, among others).

Because groundwater cannot be dated directly, only an apparent age can be obtained by using ^{3}H as a tracer—the so-called "apparent ^{3}H/^{3}He age" (e.g. Kipfer et al., 2002; Sanford, 2011). Apparent groundwater age is the measure of time since the water entered the saturated zone and was isolated from the atmosphere. Thus, the apparent age corresponds to the time since recharge has occurred (Cook and Solomon, 1995; Suckow, 2014). If dispersive and mixing effects are small, the apparent age can be compared directly with advective travel times in the groundwater system. However, long filter screens, dispersion, and flow path convergence will always lead to an age spectrum rather than an exact value. As a result, the method is typically biased toward the age of the water component with the higher tritium concentration (Kipfer et al., 2002). Moreover, the analysis is expensive, as well as labor- and time-intensive, and only a few specialized laboratories can carry out such analyses on a routine basis. Nevertheless, this method provides important information and has been successfully used in many groundwater studies (e.g. Aeschbach-Hertig et al., 1998; Corcho Alvarado et al., 2005, 2007; Ekwurzel et al., 1994; Jasechko, 2016; LaBolle et al., 2006; Manning et al., 2005; Schlosser et al., 1989; Solomon et al., 1992, 1993; Szabo et al., 1996; Visser et al., 2013).

Radiogenic ^{4}He is a by-product of the ^{3}H/^{3}He method and can be separated and used as an additional indicator for older groundwater (Lehmann et al., 2003; Solomon, 2000). ^{4}He accumulates over time due to subsurface production by radioactive decay of uranium (U) and thorium (Th) within the aquifer matrix (Solomon, 2000), and by external fluxes from the deeper strata (Torgersen and Clarke, 1985). Groundwater age determination with ^{4}He depends upon knowledge of the ^{4}He accumulation rate, which is usually obtained by comparison with ^{14}C (Torgersen and Clarke, 1985; Wei et al., 2015), ^{3}H/^{3}He ages (Beyerle et al., 1999), or from measurements of production rates obtained from aquifer material (Lehmann et al., 2003).

A newly developed, portable field-operated GE-MIMS system (Brennwald et al., 2016) provides a unique opportunity to measure dissolved gas concentrations, such as ^{4}He, in groundwater systems. Although it is not capable of providing an apparent age, the GE-MIMS system is able to measure dissolved gases in a stream of water quasi-continuously (~10–15 min) with relatively low detection limits (below 3×10^{-9} cmSTP3/g for the noble gases; Mächler et al., 2012). The GE-MIMS has been successfully used in various hydrogeological and eco-hydrological studies (e.g. Battle-Aguilar et al., 2017; Knapp et al., 2019; Mächler et al., 2012, 2013, 2014; Moeck et al., 2017b; Popp et al., 2019, 2020; Roques et al., 2020; Tomonaga et al., 2019; Weber et al., 2018).

In this study, we seek to determine the origin of groundwater and to identify spatial inter-aquifer mixing between artificially infiltrated and regional groundwater by means of a relationship between field-measured ^{4}He concentrations analyzed with the GE-MIMS system and lab-based ^{3}H/^{3}He apparent ages. The insights gained by this analysis allowed us to developed a consistent conceptual process understanding for flow and transport processes for an urban study area in Switzerland. More specifically, the following tasks are addressed:

- We aimed to determine the relationship between field-measured ^{4}He concentrations analyzed with a GE-MIMS system and lab-based apparent ^{3}H/^{3}He ages.
- The combined apparent ages from the laboratory and field measurements predicted from the aforementioned relationship will be used to evaluate the influence of artificial groundwater recharge, inter-aquifer mixing, and possible fault-induced aquifer connectivity along the flow paths.
- The results are validated with independently measured concentration patterns of water isotopes (^{18}O and ^{2}H) and hydrochemical data (cations and anions).
- We related apparent water ages, hydrochemistry, and isotope results to pollutants, such as perchloroethylene (PCE)—one of the most commonly found contaminants at the study site. Subsequently, we determined the origin of the groundwater at the observation site and drinking water pumping wells in order to aid the development of water management strategies.

2. Study area and hydrogeology

The study site is located in northern Switzerland close to the city of Basel, and covers an area of approximately 10 km^2 of mainly urban and industrial zones. The drinking water abstraction wells themselves are located in the Hardwald forest at the center of the study area (Fig. 1).

The climatic conditions are represented by an average annual precipitation of 730 mm, and a mean temperature of 11.5 °C. The surface elevation ranges from approximately 290 m above sea level (masl) in the south, to 250 masl near the Rhine River in the northeast.

Geological units present in the study area (from the bottom to the top) include the Lower Muschelkalk, Middle Muschelkalk, Upper Muschelkalk, Keuper, Jurassic strata, Tertiary sediments, and unconsolidated Quaternary cover (Fig. 2). The Lower Muschelkalk consists of marly sediments; the Middle Muschelkalk consists mainly of dolomites, marls, clays, and evaporates (*sulphate zone*); and the Upper Muschelkalk is characterized by a regionally important fractured and karstified limestone aquifer (Spottke et al., 2005). The Keuper, Jurassic strata, and Tertiary sediments represent a local aquiclude due to their low hydraulic conductivity. The bedrock units are covered by unconsolidated Quaternary sediments, which form an unconfined fluvio-glacial sand gravel aquifer (Spottke et al., 2005). The region's most prominent tectonic

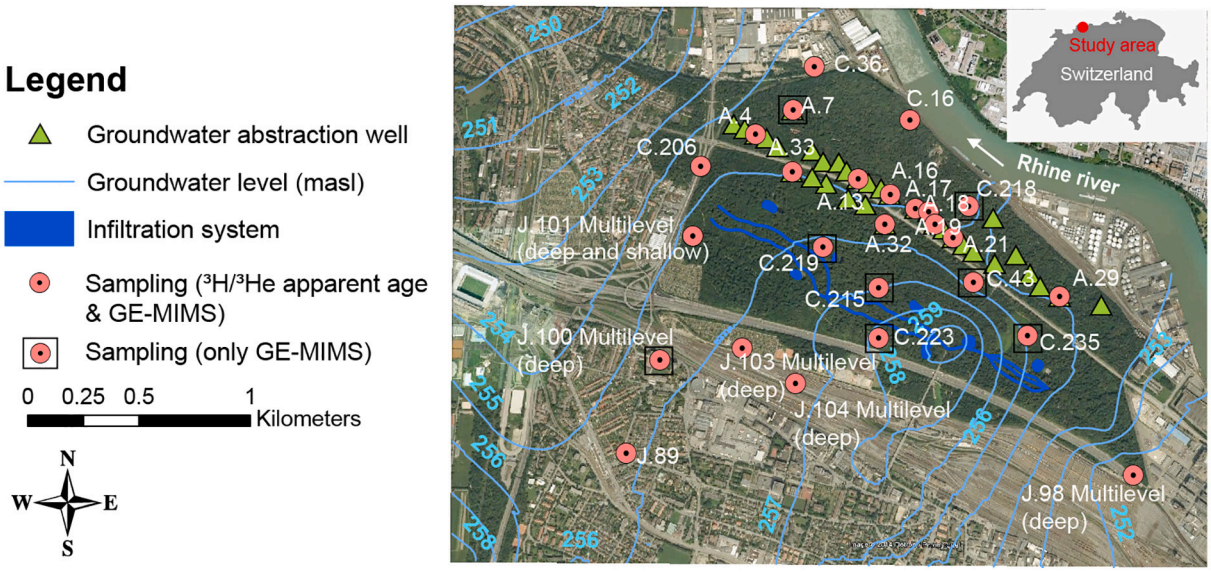

Fig. 1. Study area in north-west Switzerland with groundwater sampling locations (red circles and white text), including the Rhine River. Red circles without a black rectangle show where samples were taken for laboratory measurements, and the circles within a rectangle indicate the locations where only noble gas measurements with the GE-MIMS were carried out. Railways and industrial areas are present in the south, while industrial areas are located to the east of the Hardwald forest. Green triangles show extraction wells and artificial infiltration channels, and ponds are indicated in blue. The piezometric heads are shown as light-blue lines. (For interpretation of the references to colour in this figure legend, the reader is referred to the web version of this article.)

feature is a portion of the Upper Rhine Graben Main Border Fault, which is represented by a Flexure zone and a large number of faults (Moeck et al., 2016; Spottke et al., 2005). The hydraulic conductivity of the fractured Flexure zone is unknown and is likely spatially variable (Moeck et al., 2020). This fracture zone may represent a separate flow path due to its higher permeability and could, therefore, support the vertical exchange of groundwater, or it may be filled with fine sediments that form a hydraulic barrier (Moeck et al., 2020).

The two most hydrogeologically relevant units are the aforementioned Quaternary sediments and the Upper Muschelkalk, representing two locally important aquifers (Moeck et al., 2016, 2018b). A possible additional water component, as indicated in Popp et al. (2019), is located at the western edge of the study area (in the vicinity of the Flexure zone).

Predominant groundwater flows from southeast to northwest in the direction of the Rhine River (Fig. 1). Due to the low hydraulic conductivity of the Middle Muschelkalk (*sulphate zone*), together with the decreasing thickness of the Upper Muschelkalk, upwelling of regional groundwater from the Upper Muschelkalk into the Quaternary aquifer can occur (Moeck et al., 2016, 2018a; Popp et al., 2019).

At the study site, drinking water production is in close proximity to multiple historic landfills, as well as active industrial areas. To avoid drinking water contamination, the gravel aquifer is artificially recharged with surface water to create a hydraulic barrier between contaminated sites and drinking water pumping wells. Nevertheless, a range of pollutants, which are typically absent in the artificially infiltrated surface water, can be measured at the study site. Thus, besides being influenced by the geological structure, groundwater flow is also affected by surface water infiltration and groundwater abstraction for drinking water, as well as industrial usage and artificial recharge (Moeck et al., 2017b). The artificial groundwater recharge system with infiltration channels and ponds was designed to maintain a hydraulic gradient toward areas of potential risk, mostly in the southern direction, in which contaminated groundwater is presented (Moeck et al., 2017a). Overall, artificial recharge rates are twice as high as the pumping rates from the 33 drinking water wells (pumping well gallery) located in the sand-gravel aquifer (Fig. 1). Due to the high volume of infiltrated water (~95.000 m^3/d), a local groundwater mound has developed in the sand-gravel aquifer below the channels, serving as a kind of barrier to the natural inflow of contaminated water from adjacent areas (Fig. 1; Auckenthaler et al., 2010). Along the channels (excavated to approximately 1.5 m in depth), water from the Rhine River is diverted to recharge the aquifer and to maintain the hydraulic barrier. Water is injected at the eastern end of the channels and flows along the natural topographical gradient of the site (east to west). All water diverted into the channels infiltrates into the aquifer, with no other outflow. A mass balance approach indicated that a large proportion of the infiltration occurs close to the eastern injection point, with only about 25% of the injected water reaching the west end of the channels (Moeck et al., 2017a). Moreover, large volumes of groundwater are pumped for industrial purposes, mainly east of the study site (Moeck et al., 2020).

In the study area, various patterns of contaminants have been observed in previous studies (Moeck et al., 2016), e.g. close to landfill sites. The most commonly found contaminants are perchloroethylene (PCE), trichloroethene (TCE), hexachlorobutadiene (HCBD), and 1,1,4,4 tetrachlorbutadiene (TeCBD). There is a strong spatial correlation between the different contaminants within the study area, with a correlation of 0.84 between PCE and TCE, and 0.88 between HeCBD and TeCBD (Moeck et al., 2016). All of these compounds have a higher density than water; therefore, percolation into the subsurface can occur.

A common hypothesis is that the presently observed concentrations of PCE and TCE are released from adjacent former landfills south of the pumping water gallery (Auckenthaler et al., 2010; Moeck et al., 2016). The bedrock underlying these former landfills consists mainly of limestone from the fractured Muschelkalk formation. Fractured bedrock aquifers with minimal or no overburden cover are highly vulnerable to contamination (Levison et al., 2012; Palau et al., 2014). Aquifer contamination to a depth of 100 m can be found in groundwater samples at the study site (Auckenthaler et al., 2010). Overall, the highest concentrations of chlorinated hydrocarbons were detected in the south and southwestern part of the study area (Moeck et al., 2016). Regional groundwater with higher concentrations of chlorinated hydrocarbons is, therefore, most likely to originate from the south (Moeck et al., 2016). Consequently, it is important to understand the subsurface processes to develop groundwater protection plans and secure safe drinking water production.

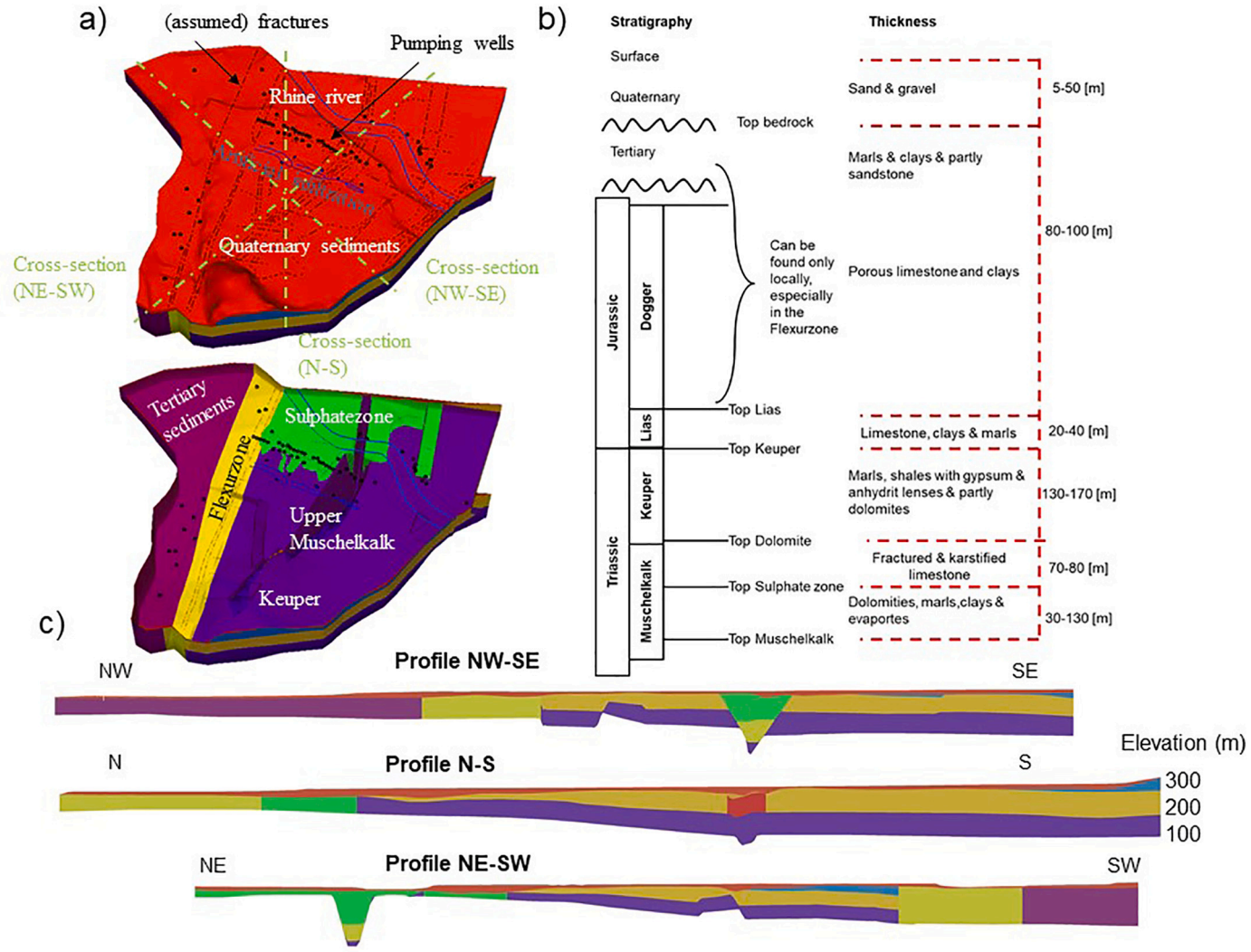

Fig. 2. a) Geological units with pumping well locations (black points), the Rhine River and artificial infiltration system (blue lines), and (assumed) fractures (dashed lines). The top panel shows the Quaternary sediments where for the bottom panel the Quaternary sediments are hidden. b) Simplified stratigraphic profile (not to scale) with the thicknesses of the different geological units indicated. c) Cross-section view for three profiles. (For interpretation of the references to colour in this figure legend, the reader is referred to the web version of this article.)

3. Data and methods

We analyzed a set of environmental tracers, collected mostly between 2015 and 2017. Sampling locations consist of 16 groundwater observation wells (which includes six multilevel wells) and 11 pumping wells (Fig. 1). For the sampling of the wells, we either used preinstalled pumps at the pumping wells or a submersible pump (MP1, Grundfos) in case of observation wells. We started sampling after purging all wells three times their volume and after field parameters (O_2, electrical conductivity (EC), temperature, and pH) had reached a stable level (i.e. at least three consecutive measurements with the same concentrations within analytical uncertainty were obtained after analysis with a calibrated HACH HQ40D portable multimeter). The different well screen depths for the multilevel wells were sealed with an inflatable double packer system and thus we assume that wellbore flow is negligible. All sampled well locations of the drinking water site and well depths are provided in Table 1. Out of the 27 observation wells, 15 wells are screened in the Quaternary aquifer whereas 12 screens are located in the Muschelkalk aquifer. During our sampling campaigns, the managed aquifer recharge system was operated under standard conditions (i.e. average water infiltration and abstraction rates, which govern the hydraulic head distribution). Thus, hydraulic conditions representative of the standard operation of the managed aquifer recharge site were guaranteed.

3.1. Hydrochemical data, water isotopes, and PCE concentration

All cations and anions, as well as stable water isotopes (^{18}O and ^{2}H), from samples acquired during the field campaigns were analyzed at Eawag labs. Triplicate measurements and blanks were used, but the results were very stable and no data drift was observed. The chemical analysis of the 27 samples was performed using standard methods and devices for the major cations and anions (Metrohm 761 Compact IC). Only datasets with a charge balance error under 5% were used for the hydrochemistry analysis and interpretation. Güler et al. (2002) stated that a calculated charge balance under 5% is an acceptable error. The hydrochemistry data were used to assess the hydrogeological origin of the groundwater (e.g. limestone or sand-gravel aquifer). In addition, 26 samples were analyzed for stable isotopes (^{18}O and ^{2}H) with a Picarro L1102-I. Furthermore, 27 sampling locations were analyzed in the accredited cantonal laboratory to provide PCE data.

Table 1
Sampling locations with coordinates, relative and absolute depths, measured $^{3}H/^{3}He$ apparent age, gas equilibrium membrane inlet mass spectrometer (GE-MIMS) measurements, and stable water isotope, perchloroethylene (PCE), and hydrochemical data (cations and anions).

ID	Type	X	Y	Relative depth (m)	Absolute depth (masl)	$^{3}H/^{3}He$ apparent ages (years)	^{4}He (ccSTP/g)	EC (μS/cm 20 °C)	Chloride (mg/L)	Sulfate (mg/L)	Na (mg/L)	Ca (mg/L)	HCO_3 (mg/L)	^{18}O (‰)	^{2}H (‰)	PCE (μg/L)	Aquifer
A.13	Pumping well	615407	266156	38.5	234.5	1.5	4.50E-08	322	8.6	26	7.1	52.9	175.9	−11.24	−81.58	0.15	Quaternary
A.16	Pumping well	615551	266088	41.3	231.3	1	4.21E-08	311.4	9.8	27	7.4	51.2	164.1	−11.2	−80.71	0.1	Quaternary
A.17	Pumping well	615665	266022	37.1	237.1	2.5	4.70E-08	404	9.6	66	8.2	70.4	184.2	−11.28	−81.62	0.11	Quaternary
A.18	Pumping well	615725	266009	38.21	234.6	0	4.94E-08	324.7	9.9	32	7.5	54.1	165.9	−10.99	−78.9	0.1	Quaternary
A.19	Pumping well	615752	265951	40.19	232.75	1	4.42E-08	311.8	9.8	26	7.1	51.3	163.5	−11.2	−80.8	0.07	Quaternary
A.21	Pumping well	615835	265894	37.1	237.1	0	4.60E-08	319	8.1	25	6.9	52.7	178.1	−11.32	−82.34	0.07	Quaternary
A.29	Pumping well	616314	265628	37.3	237.5	0.2	5.00E-08	323	8.3	24	6.9	53.6	179.7	−11.18	−81.52	0.12	Quaternary
A.32	Pumping well	615528	265953	28.7	240.83	0	5.10E-08	315	8	25	6.5	52.1	173.3	−11.22	−81.19	0.07	Quaternary
A.33	Pumping well	615110	266190	40.2	232.2	11.7	6.30E-08	433	12.4	75	12.1	73.3	185.4	−11.2	−80.84	0.11	Quaternary
A.4	Pumping well	614947	266357	39.7	231.7	12.3	5.50E-08	365	11.2	29	9.8	59.8	199.7	−11.16	−81.52	0.22	Quaternary
A.7	Pumping well	615114	266466	26.1	243.9	8.2	9.50E-08	510	19.3	84	20.6	81.4	217.2	−11.11	−80.67	0.24	Quaternary
C.16	Piezometer	615639	266422	25.3	241.1	3.1	4.90E-08	350	10.9	36	8.5	57.2	181.2	−11.01	−80.28	0.39	Muschelkalk
C.206	Piezometer	614700	266215	29	243.2	36.6	3.80E-07	723	39.4	73	33.5	114.9	342.6	−9.78	−70.75	0.75	Muschelkalk
C.215	Piezometer	615500	265667	27.5	244.3	2.3	4.20E-08	296	8	24	6	49.4	160.7	−11.12	−81.23	0.01	Muschelkalk
C.218	Piezometer	615905	266035	–	–	4.3	6.00E-08	362	7.9	24	7.4	62	209.2	–	–	0.19	Quaternary
C.219	Piezometer	615250	265850	20	253.7	3.1	4.90E-08	300	8	24	6.1	49.5	162.8	−11.14	−81.09	0.07	Muschelkalk
C.223	Piezometer	615500	265440	26	247.3	2.8	4.60E-08	315	8.1	25	6.1	53.2	173.4	−10.89	−80.25	0.01	Quaternary
C.235	Piezometer	616170	265451	31.5	242.9	3.5	5.30E-08	320	7.9	24	7.2	53.3	180.6	−10.88	−80.13	0.06	Quaternary
C.36	Piezometer	615208	266660	24.3	238.5	25.6	2.00E-07	627	31.5	122	29.5	99.4	234.2	−8.76	−66.02	0.25	Muschelkalk
C.43	Piezometer	615925	265692	33	240.9	3.3	5.10E-08	304	7.6	23	6.3	51.2	169.3	−8.81	−65.63	0.08	Muschelkalk
J.100 (deep)	Multilevel well	614515	265341	76.2	198.6	18.7	1.90E-07	1017	56	118	55.1	144.4	484.7	−11	−80.12	0.32	Muschelkalk
J.101 (deep)	Multilevel well	614665	265901	45.2	227.7	8	9.30E-08	636	18.8	46	13.4	113.6	356.4	−11.32	−82.54	1	Muschelkalk
J.101 (shallow)	Multilevel well	614665	265901	19	253.9	4.1	7.50E-08	566	14.6	41	9.6	107.4	316.1	−11.25	−82.08	0.98	Quaternary
J.103 (deep)	Multilevel well	614885	265397	54	220.1	6.1	7.79E-08	386	11.9	33	9.7	10.7	218.1	−11.06	−80.82	1.2	Muschelkalk
J.104 (deep)	Multilevel well	615125	265237	68	207.5	2.3	4.81E-08	381	15.48	41.44	13.2	10.3	202	−8.94	−66.71	0.15	Muschelkalk
J.89	Piezometer	614365	264925	70	209.1	58	4.85E-07	938	58	127	38.2	139	386.9	−10.04	−73.35	3.6	Muschelkalk
J.98 (deep)	Multilevel well	616643	264826	80	188.8	13.5	1.36E-07	393	15.24	44.15	9.4	13.5	210.4	−8.96	−65.81	0.51	Muschelkalk

Predicted age based on GE-MIMS and $^{3}H/^{3}He$ apparent age relationships (see Fig. 3).

3.2. Laboratory-based noble gas analysis and $^3H/^3He$ dating

For the laboratory-based noble gas analysis, we collected 18 water samples (Fig. 1) in copper tubes following standard sampling procedures (Beyerle et al., 1999, 2000). The tube volume was exchanged several times before the actual sampling was conducted. The samples were analyzed for noble gases at the ETH noble gas lab in Zurich (Switzerland), as described by Beyerle et al. (1999). We determined tritium concentrations using the ^{3}He in-growth method (Tolstikhin and Kamenskiy, 1969). The copper tubes were stored for several months after the gas (^{3}He) extraction to allow for the accumulation of ^{3}He from tritium decay (Beyerle et al., 1999, 2000). We used the closed-system equilibrium model (Aeschbach-Hertig et al., 2000) implemented in the numerical code NOBLE90 (Peeters et al., 2003) to obtain $^3He_{trit}$. For a detailed description on the analysis of dissolved noble gases and tritium in water, see Beyerle et al. (2000).

3.3. On-site noble gas analysis

In the field, we use the newly developed GE-MIMS (Brennwald et al., 2016, Gasometrix GmbH, Switzerland) to obtain dissolved ^{4}He concentrations. The sampling and measurement procedure is explained in detail in Popp et al. (2019) and will, thus, be only briefly summarized. The abstracted water is pumped through a membrane module (3 M Liqui-Cel, 2017), where the dissolved gases are extracted into a head space until a gas-equilibrium between the dissolved and the free gas phase is established (Brennwald et al., 2016). The module is connected via a small capillary to a quadrupole mass spectrometer for final gas analysis. Air-water equilibrium within the membrane module is reached after 10–15 min. We sampled the ambient air, which we used as the standard. We conducted four measurement cycles (for both the air standard and dissolved gas measurements), which resulted in an overall sampling time of less than 60 min at each sampling location. Water temperature was continuously recorded before the membrane module (DS18B20 Maxim temperature probe). This allows the conversion of the determined gas partial pressures into dissolved gas concentrations according to the solubility constants of Henry's law at the respective water temperatures assuming zero salinity (Kipfer et al., 2002). For a more comprehensive description of gas analysis using the GE-MIMS system, see Brennwald et al. (2016).

3.4. Combining $^3H/^3He$ dating and on-site noble gas analysis

^{4}He accumulation rates are often obtained from $^3H/^3He$ ages, and it has been shown that ^{4}He concentrations measured using laboratory and field-based (GE-MIMS) methods closely agree (Battle-Aguilar et al., 2017; Popp et al., 2019). Therefore, it can be postulated that a relationship between field-measured ^{4}He and $^3H/^3He$ apparent ages can also be derived in this manner. Hence, a relationship between ^{4}He concentrations measured in the field with the portable GE-MIMS system and laboratory measured $^3H/^3He$ apparent age would deliver certain advantages, even though laboratory data are still required to establish this relationship. The advantages are that ^{4}He GE-MIMS field measurements are less expensive and easier to obtain, and thus more groundwater observation points can be sampled in a relatively short period of time. In this study, apparent ages can be derived based on a linear regression between laboratory $^3H/^3He$ apparent age data and field-measured ^{4}He concentration data.

4. Results

4.1. Relationship between $^3H/^3He$ apparent ages and GE-MIMS measurements and spatial distribution

A linear relationship between the field-based ^{4}He concentrations collected with the GE-MIMS system and the estimated laboratory $^3H/^3He$ apparent ages is shown in Fig. 3. The ^{4}He from the field measurements correlates well with the laboratory $^3H/^3He$ apparent ages, resulting in a Pearson correlation of 0.93. The residuals have a mean (standard deviation) of −0.16 (3.0) years. The residuals are randomly distributed and no distinct trend in the distribution of points is observed, indicating the suitability of the linear regression in explaining the data. Most data fall within the 95% confidence interval. Only pumping wells A.4 and A.33, as well as observation well C.36 (all located in the northwestern region of the study area), are not within the intervals. Results from analyzing the regression shows that outliers are well A.4 and A.33, wells with high leverage and influential observations are C.206 and J.89. The results from this analysis and the link to the hydrogeological system are discussed in Section 5.

Using the linear regression equation, apparent ages can be predicted for sampling locations where only ^{4}He concentration from the GE-MIMS measurements are available. The predicted ages are all less than 10 years, except for the deep sampling location of the multilevel well J.100, in which an age of 18.7 years was predicted. In this data range, the confidence interval width, the range of plausible values for the unknown age is smaller than for the upper part where larger ^{4}He concentrations are measured and only a few observations with both $^3H/^3He$ apparent ages and ^{4}He concentrations exist (e.g. J.89 and C.206). Factors affecting the confidence interval width include the size of the sample, the confidence level, and the variability in the samples. A larger sample set with small variability for a specific value range will tend to produce a better estimate of the predicted apparent age and lower uncertainty. This is indicated in Fig. 3 where predicted age (red rectangles) are located where most observations with both $^3H/^3He$ apparent age and ^{4}He concentrations exist. Thus, uncertainty in the predicted age would be higher for higher ^{4}He values.

Due to the relationship between $^3H/^3He$ apparent age and ^{4}He, the question of why both measurements correlate so well arises. One possible explanation is that radiogenic helium is accumulated in the aquifer by radioactive decay of U and Th within the aquifer matrix; therefore, the ^{4}He concentration is controlled by the residence time of the groundwater in the aquifer. Another explanation is that high ^{4}He is controlled by excess air. Entrapment and dissolution of air bubbles, in response to water-table fluctuations or groundwater recharge, leads to the formation of excess air, i.e., a surplus of atmospheric gases relative to atmospheric solubility equilibrium (Kipfer et al., 2002). Naturally occurring groundwater typically has higher excess air, where low excess air should be present in the young artificial infiltrated surface water where a large amount of water is infiltrated daily (~95.000 m^3/d). A mixing between the older naturally occurring groundwater and young infiltrated water could also explain the correlation.

To understand the reason for this inter-relationship, we compare measured argon (Ar) with total He concentrations (Fig. 4). Ar concentration is not affected by ^{4}He accumulation in the aquifer, but only by excess air processes. In the case of a correlation between Ar and ^{4}He, it is assumed that excess air is controlling the relationship between $^3H/^3He$ apparent age and ^{4}He; whereas, if Ar does not vary with the ^{4}He concentration, then the ^{4}He accumulation in the aquifer leads to the $^3H/^3He$–^{4}He relation. Fig. 4 shows that Ar varies in a relatively narrow range and does not show a correlation with He. Thus, the accumulation of ^{4}He in the aquifer by the radioactive decay of U and Th leads to a strong correlation between $^3H/^3He$ apparent age and ^{4}He.

Observation wells C.206, C.36, and J.100 (deep), which have higher ^{4}He concentrations, are all located at the western edge of the study area in the vicinity of the Flexure zone. These wells will be discussed in detail in the following sections. Moreover, a stratification can be observed, where deeper sampling locations show a slightly higher He concentration (e.g. J.101 deep and shallow sampling depth). Moreover, wells (e.g. A.7, A.33), indicating higher ^{4}He concentrations compared to most other wells used for drinking water supply.

The spatial distribution of both laboratory-measured $^3H/^3He$ apparent ages and field-based predicted ages (hereafter called "apparent

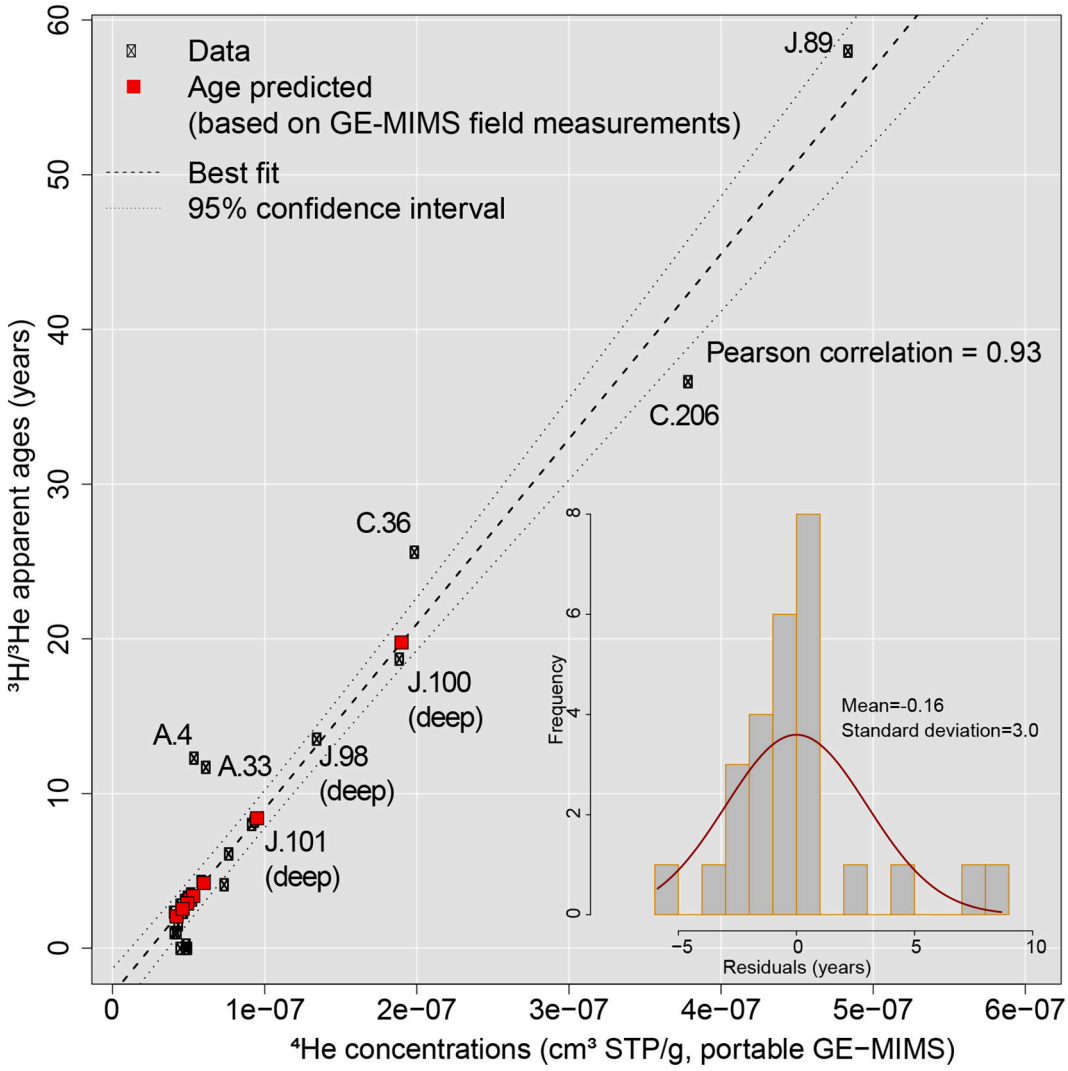

Fig. 3. Relationship between the field-measured ^{4}He concentrations acquired with the portable gas equilibrium membrane inlet mass spectrometer (GE-MIMS) and the estimated laboratory $^{3}H/^{3}He$ apparent ages (years). Black rectangles represent the data where both laboratory and GE-MIMS field-based data were available. Red rectangles show the predicted apparent ages based on the estimated linear relationship. The graph on the bottom-right shows the residuals with a mean (standard deviation) of −0.16 (3.0 years). (For interpretation of the references to colour in this figure legend, the reader is referred to the web version of this article.)

age" for measured and predicted) is provided in Fig. 5. The spatial distribution shows a distinct trend, where relatively young water is mostly located close to the artificial infiltration system and the oldest water (58 years; observation well J.89) is found in the south close to a landfill where Muschelkalk is present. At the western edge of the study site, for instance, groundwater that most likely represents the regional flow path mixed with younger infiltrated water can be found and, thus, a mixed water age is obtained (older than the artificial infiltrated water, but younger than the assumed regional groundwater). At the western (e.g. J.100) and eastern (e.g. J.98) edges of the study area, the decreases in artificial infiltration result in older water ages. Interestingly, observation well C.206 also shows a relatively old groundwater age (36.6 years). At most multilevel wells, an increasing trend in apparent ages with increasing depth can be observed. For example, for observation well J.101, an apparent age of 4.1 years was estimated for the upper sampling screen, with an increase to 8.0 years of age for the lower sampling screen. The observation wells in the direct vicinity of the artificial infiltration system show an age $>$ 2.3 years; whereas, at the pumping wells, the age is younger. At the pumping wells, older ages can be observed for wells A.33, A.4, and A.7—all of which are located at the western edge of the pumping well gallery. Although pumping well A.17, which is centrally located in the well gallery, shows an older age of 2.5 years, all other pumping wells show younger apparent ages.

4.2. *Hydrochemistry and water isotopes*

To better constrain the age distribution, hydrochemistry data (namely cations and anions) were additionally used to provide an indication about the origin of the sampled groundwater. The groundwater in the quaternary aquifer shows the same hydrochemistry than the artificial infiltrated surface water (Moeck et al., 2016). In contrast, the Muschelkalk water has a considerably different hydrochemistry than the artificial infiltrated surface water, including an increase in Ca^{2+}, Na^{+}, Cl^{-}, SO_4^{2-}, and HCO_3^{-} at the study site (Moeck et al., 2016, 2018b), such that a relationship between hydrochemistry and apparent age is expected. Fig. 6 shows a strong relationship between the cations Na^{+} and Ca^{2+}, as well as the anions Cl^{-} and HCO_3^{-}, with apparent age. Note that a correlation between EC and SO_4^{2-}, respectively, with apparent age results in a correlation of 0.79 in both cases, but is not graphically presented here. A distinct trend between the hydrochemical data and the apparent age can be observed, where older groundwater shows a higher concentration of the aforementioned cations and anions (e.g. J.89).

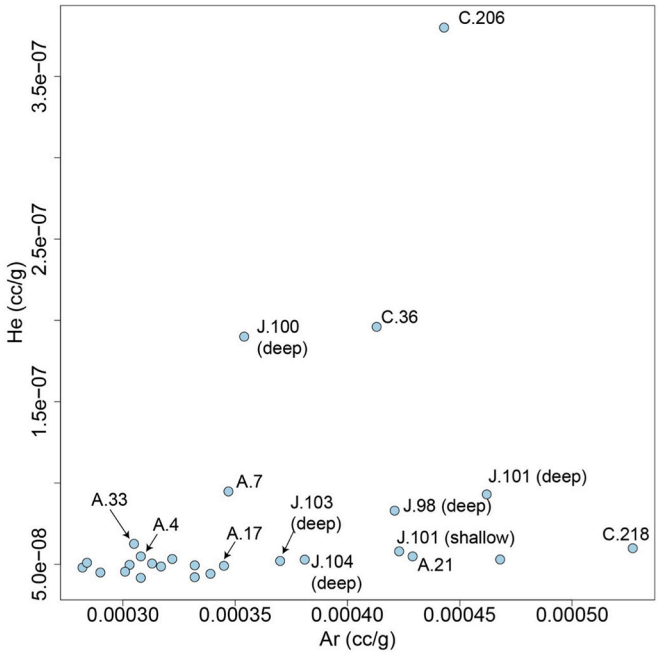

Fig. 4. Ar (cc/g) versus total He (cc/g) plot.

Again, a trend between sampling locations in the south (J.89), following the regional flow path along the western edge (C.206) toward the north (C.36), can be observed. At pumping wells where the impact of artificial infiltration is low (e.g. A.7), a higher concentration of cations and anions can be observed. Furthermore, stratification at the multilevel wells is also present, where greater age and deeper sampling intervals correlate to higher concentrations (J.101), although the differences are not large.

Stable water isotopes (^{18}O and ^{2}H) ranged from −11.32 to −8.76‰ and − 82.54 to −65.63‰, respectively (Fig. 7). The isotope compositions follow the local meteoric water line. Sampling locations in the south and at the western edge (J.89 and C.206) show different isotope values than most of the other locations, which presents an isotopic signature from the artificially infiltrated Rhine surface water. The groundwater multilevel well (J.98), as well as the sampling locations in the north-west (C.43 and C.36), have an enriched isotope composition, indicating different water sources. The measured values cannot be explained by the variability in Rhine water used to recharged the gravel aquifer (Range of Rhine water isotopes (time series of 5 years) is between −11.4 and − 10.3‰ for $\delta^{18}O$ and − 81.8 and − 74.1‰ for $\delta^{2}H$). This interpretation is further underpinned by combining the apparent age with ^{18}O. Again, sampling locations J.89 and C.206 show a distinctly different age and isotope composition. Also, locations C.43, C.36, and J.98 are clearly differentiated from most other samples, which are plotted in a very narrow range of ages and isotope values.

4.3. Linking apparent age, water origin, and PCE concentration

The PCE contamination used as a proxy for many other contaminants found at the study site is related to information about the apparent age distribution and groundwater origin. Fig. 8 shows the linkage between the apparent ages and PCE concentrations. The highest concentration of PCE (3.6 μg/L) occurs where the oldest groundwater was estimated (58 years; J.89), located in the south and in close vicinity of a landfill. In addition, observation wells C.206 and C.36 underpin the relationship between age and PCE concentration, where the PCE concentration decreases with decreasing age. Moreover, most multilevel wells with deeper sampling depths indicate higher concentrations of PCE. This might highlight the higher density of PCE than water, with percolation into the deeper subsurface occurring. Additionally, groundwater stratification can be found where younger surface water has likely infiltrated the upper part of the aquifer, and older water with a higher fraction of regional Muschelkalk groundwater can be found in the lower part. In addition, the pumping wells in the western part of the pumping well gallery (e.g. A.4 and A.7) show higher concentrations of PCE; although, the concentrations are relatively low overall at the pumping wells. In general, for sampling locations where water ages are lower, the PCE concentrations are also typically lower.

To better constrain the relationship between PCE, apparent age, and water origin, we used results from a previous Bayesian groundwater-mixing model developed for the study area (Popp et al., 2019). This approach explicitly considers the possibility of unknown end-members (referred to as “residual end-member”). The Bayesian model defined two end-members that represent the infiltrated Rhine surface water and regional groundwater sampled from observation well J.100 (deep sampling screen).

Observation well J.100 is to be found in the southwestern edge of the study area, a location where the Muschelkalk strata is present (Moeck

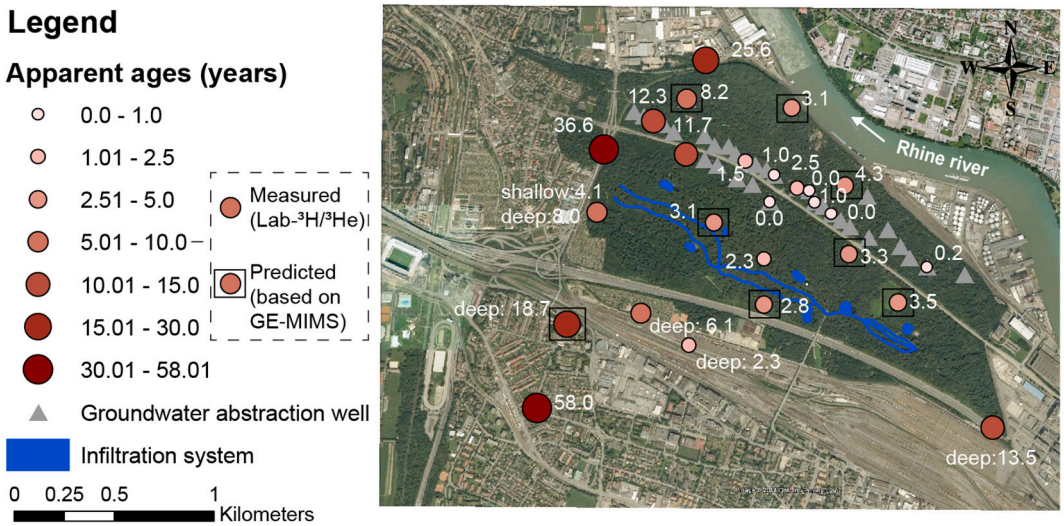

Fig. 5. Apparent age (years) distribution of groundwater in the study area. Predicted ages are shown with a black rectangle around the sampling location. The size and colour of the circles show the apparent ages: small white circles represent young ages and larger dark red circles represent older ages. (For interpretation of the references to colour in this figure legend, the reader is referred to the web version of this article.)

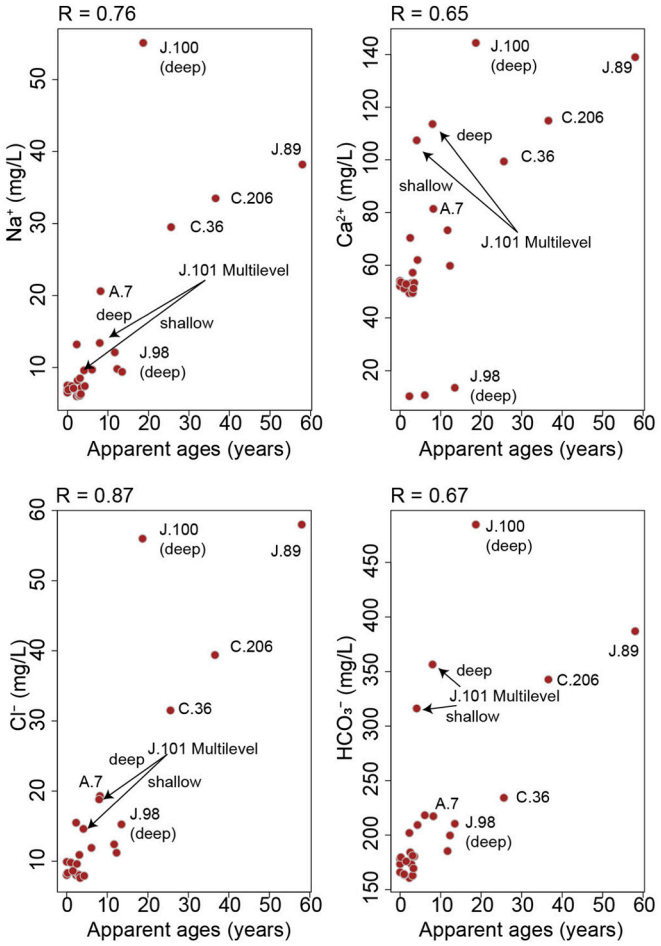

Fig. 6. Apparent age (years) versus cation and anion concentrations (mg/L).

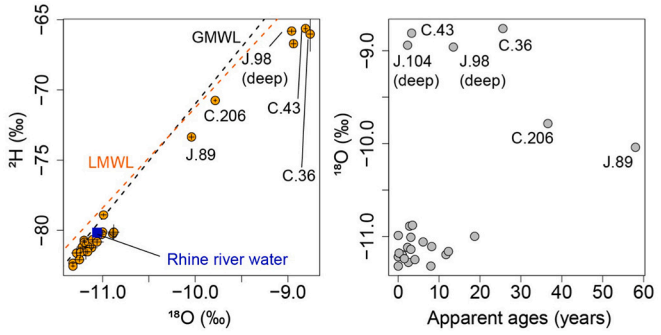

Fig. 7. Left panel: $\delta^{18}O - \delta^{2}H$ (‰) plot for the study area. The black line shows the global meteoric water line (GMWL) and the dashed orange line shows the local meteoric water line (LMWL). Although just one sample of the Rhine water is shown, the range of Rhine water isotopes (time series of 5 years) is between −11.4 and − 10.3‰ for $\delta^{18}O$ and − 81.8 and − 74.1‰ for $\delta^{2}H$. Right panel: $\delta^{18}O$ (‰) – apparent age (years) plot for the study area.

et al., 2016). In addition, groundwater level observations indicate that this well is hardly affected by the artificial infiltration, the isotopic composition is indicative of Muschelkalk water (Moeck et al., 2016) and therefore can be assumed to be representative for the regional groundwater (Popp et al., 2019).

The Bayesian model was run with a tracer set, which includes ^{4}He analyzed on-site to determine mixing ratios in the groundwater. Fig. 9 shows the apparent age versus the fraction of the corresponding end-member from the mixing calculations. The size of the points represent

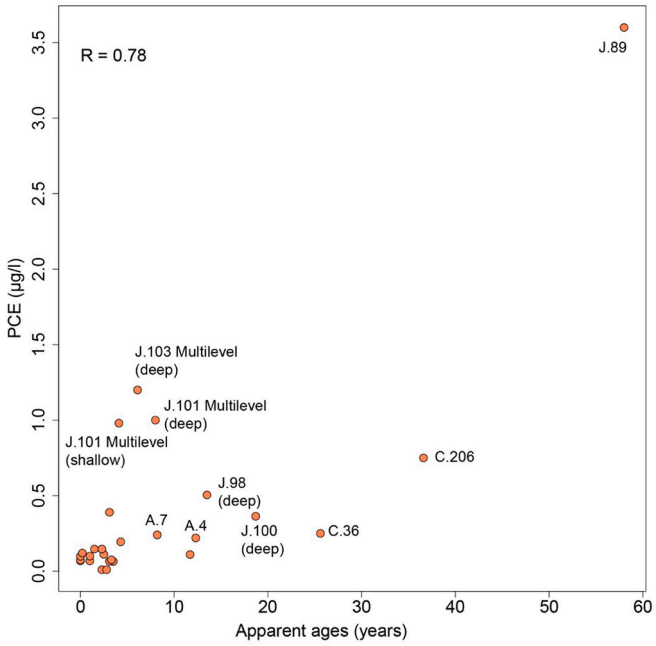

Fig. 8. Apparent water age (years) versus measured PCE concentration (µg/L) with a Pearson correlation of 0.78.

the PCE concentration at the sampling locations. If the proportion of infiltrated water is high, then both PCE concentrations and apparent ages tend to be low. In the Rhine surface water, PCE is typically absent and artificial infiltrated water is, thus, free of such contaminants. For pumping wells with a slightly smaller fraction of surface water (e.g. A.17, A.4, and A.7), the apparent age and PCE concentrations increase. For high and deep wells (e.g. J.101), the fraction of surface water is low and PCE concentrations are around 1.0 µg/L. For these wells, it seems that a proportion of the residual end-member is contributing to the water chemistry, age, and PCE concentration. Beyond that, we see that observation well C.206 has a high proportion of both Muschelkalk and residual groundwater, leading to a PCE concentration of 0.75 µg/L and an age of 36.6 years. The presence of a high ratio of a previously unknown water source (Flexure zone with fractures) suggests that faults can play a role as preferential flow paths for the transport of old groundwater, contributing to PCE contamination. The typically unknown fracture network and distribution, however, makes a tracking of the PCE origin extremely challenging (e.g. Palau et al., 2014; Perrin et al., 2011; Therrien and Sudicky, 1996; Slough et al., 1999). However, the highest PCE concentration was measured at observation well J.89 (3.6 µg/L) having the oldest age (58 years) and is located in the direct vicinity to a former landfill.

5. Discussion

Using $^{3}H/^{3}He$ apparent ages provides important information for site characterization and helps to develop conceptual models for groundwater flow and transport processes. However, the analysis is expensive and time- and labor-intensive. Only a few specialized laboratories can carry out such analyses on a routine basis, potentially limiting the amount of sampling locations (Popp et al., 2019). In contrast, the new developments in field-based, portable mass spectrometry provide a unique opportunity to measure dissolved gas concentrations, such as ^{4}He or other noble gases, relatively quickly (Battle-Aguilar et al., 2017; Brennwald et al., 2016, 2020). Due to the quasi–real-time measurements in the field, adaptive and more efficient sampling campaigns can be carried out. The two methods, laboratory-based $^{3}H/^{3}He$ apparent age estimation and ^{4}He concentrations based on in-situ GE-MIMS

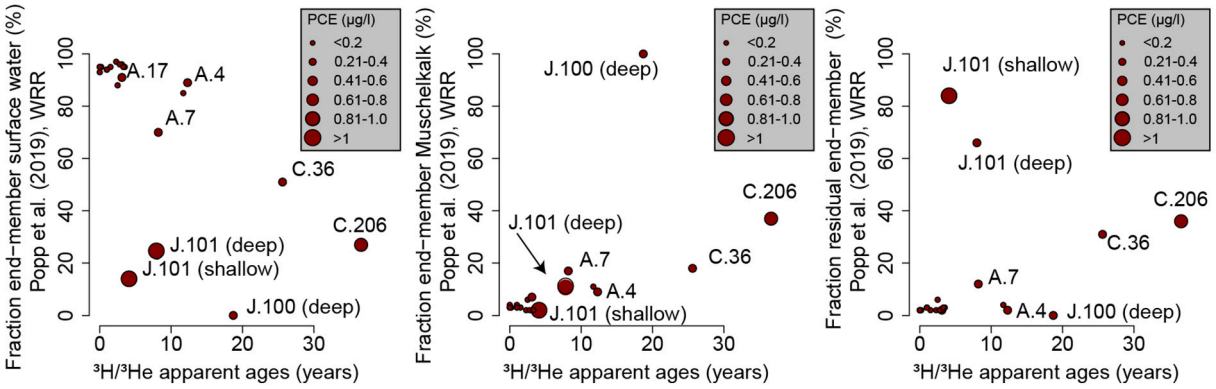

Fig. 9. Left panel: apparent age (years) and fraction of artificial infiltrated Rhine surface water (%); middle panel: apparent age (years) and fraction of Muschelkalk water (%); and right panel: apparent age (years) and fraction of residual (unknown, possible third groundwater type) groundwater (%). The size of the circles represents the PCE concentration (µg/L): smaller circles indicate small PCE concentrations and larger circles indicate larger PCE concentrations. Note that for wells C.218, J.89, and J.98, no mixing fractions are reported in Popp et al. (2019).

measurements, however, differ regarding sampling volume and technique, analytical procedure, calibration, and data processing. Thus, the assumption that both methods yield comparable results is not straightforward. However, as demonstrated in this study and elsewhere (Battle-Aguilar et al., 2017; Popp et al., 2019), a statistical correlation between data sets can be derived, demonstrating that the results of the simpler GE-MIMS system are as satisfactory as those of the highly sophisticated lab-based method. Thus, the combined use of laboratory and predicted groundwater apparent ages (based on the GE-MIMS relationship) opens new opportunities in determining groundwater sources and apparent ages. This allows increased insight into the flow and transport behavior of contaminants, and helps to determine groundwater residence times. Moreover, the GE-MIMS is able to measure various gases, and might provide further opportunities to investigate a study site from additional perspectives (Knapp et al., 2019; Popp et al., 2020; Roques et al., 2020; Tomonaga et al., 2019). Moreover, we can demonstrate that the relationship between $^{3}H/^{3}He$ apparent ages and ^{4}He concentrations is controlled by radiogenic He, which accumulates in the aquifer by radioactive decay of U and Th and, thus, ^{4}He concentration is mainly controlled by the residence time of the groundwater in the aquifer.

At the study site, the combined use of measured and predicted apparent ages linked to hydrochemical data, water isotopes, and PCE concentrations were a valuable toolset to identify spatial inter-aquifer mixing in the subsurface. The results obtained from the age distribution analysis are strongly supported by the information gained from the isotopic and hydrochemical data. Based on the combined results, it can be concluded that in the vicinity of the pumping wells, a higher amount of artificially infiltrated surface water is mixed with water originating from the regional flow pathway. The mixing signal can also be found in a few specific pumping wells in the western part of the study area, which seems to be linked to fault-induced aquifer connectivity. The Flexure zone, with its large number of faults, represents a separate flow path (as indicated by Popp et al., 2019). Moreover, it is indicated that close to the infiltration system upwelling of regional groundwater through fractures occurs. This upwelling causes mixing between the young artificial infiltrated water and older regional groundwater leading to higher ages in the vicinity of the infiltration system (Fig. 5). This is in line with results obtained from the spatial concentration pattern of the persistent artificial sweetener acesulfame (Moeck et al., 2017b), which shows a significant decrease in concentration in the wells compared to the infiltrated water, especially in an area close to the infiltration channels. In this area, upwelling through the fractures might have been localized, and a contribution from the limestone aquifer—which has smaller concentrations of acesulfame—may dilute the groundwater in the upper aquifer (Moeck et al., 2017b). This upwelling can occur locally which is demonstrated by Popp et al. (2019). It was shown that further away from the artificial recharge system, (e.g. A.16), the fraction of Rhine filtrate is still large and the apparent age is small (1 year). For the pumping well A.17 which is in 130 m distance, we showed that a comparatively lower fraction of recently infiltrated water exists and that the apparent age increases (2.5 years). Moreover, three dimensional modeling for the study area suggests further that within the well field, the central pumping wells (e.g. pumping well A.17) could be extracting more regional groundwater (Moeck et al., 2020). On the other hand, Moeck et al., 2017b showed that with constant pumping rates, more artificially infiltrated surface water is extracted, which led to a higher dilution of the regional groundwater. We postulate that the combined effect of upwelling of regional groundwater and constant pumping explain that the youngest groundwater is in part associated to pumping wells and not to observation wells near the infiltration facilities. Thus, water mixing through the Flexure zone and fractures might be of greater importance for water management at the study site than previously assumed. Wells located at the western edge of the study area (i.e. 21.C.36, 21.A.7, 21.C.206, 21.J.101: shallow and deep) show elevated ^{4}He concentrations and higher ages (from 4.1 to 36.6 years). Although, wells A.4 and A.33 are identified as outliers in the regression analysis, we observed that the northwestern part of the study area is less impacted by the artificial recharge and the fraction of Rhine filtrate decreases. All wells with a considerable fraction of the residual end-member (see also Fig. 9) are being located at the western border of the study area and therefore it might indicate a different hydrogeological flow dynamic. Here, another regression model might be useful but building a linear regression only on a few observations points would not lead to a robust model. Moreover, groundwater age was found to increase with depth (e.g. multilevel well J.101 exhibited an age of 4.1 years and 8.0 years for the upper and lower sampling screens, respectively) and distance to the artificial infiltration system (e.g. J.98 and J.89). Furthermore, a large proportion of the infiltration occurs close to the eastern injection point, with only about 25% of the injected water reaching the west end of the channels (Moeck et al., 2017a, 2020). Thus, the local groundwater mound in the sand-gravel aquifer, which serves as a barrier to natural inflow of potentially contaminated water from adjacent areas, is spatially imbalanced, and more regional groundwater is expected at the western edge of the sample site. This can also be observed by considering the PCE concentration and groundwater age, which is higher at the western edge.

Generally, the highest PCE concentrations can be found in the south (in the vicinity of the landfill; observation well J.89) and west (e.g. observation well C.206), where the impact of artificial infiltration is low. Well C.206 was identified in Moeck et al. (2016) as an exception based on a multicomponent statistical analysis. This sampling location situated in the vicinity of the Rhine Valley Flexure zone differs compared to other wells in terms of high concentrations of Na^{+}, K^{+}, Ca^{2+}, Mg^{2+}, HCO^{3-},

SO_4^{2-} and Cl^- (Moeck et al., 2016, 2017a, 2017b). Popp et al. (2019) showed that C.206 has an exceptionally low fraction of the surface water end-member but simultaneously also has a relatively high fraction of an unknown end-member. It was speculated that this might be an indication of vertical exchange and upwelling of waters originating from the salt and gypsum layer (Moeck et al., 2016). The wells J.89 located in the south of the study area has the oldest water and highest concentration of PCE. This well shows a strong impact of regional limestone water. These afromentioned two wells (J.89 and C.206) are important because they not only have a high PCE concentrations and highest apparent ages, but they also have a disproportionate impact on the regression. For instance, if we would drop one of these observations, it would affect our model. Thus, it is important to have these values included and if possible to acquire more data with large apparent ages and ^{4}He concentrations. This is, however, difficult for most studies because typically it is not known where these locations are. Thus, a sound initial conceptual process understanding for flow and transport must be developed before sampling in the field is carried out. Small concentrations of PCE can be found at all pumping wells, but are slightly higher for wells at the western edge. However, pumping well A.17, located more centrally in the pumping gallery, was found to exhibit different hydrochemistry, age, and PCE concentrations compared to most other wells in the same vicinity. This well seems to be hydraulically connected to the underlying aquifer as already indicated in previous studies (Moeck et al., 2016, 2017b; Popp et al., 2019). According to Popp et al. (2019), differences at this well might originate from a higher fraction of regional groundwater (6%) and residual (most likely fracture) end-member (6%) relative to the surrounding wells. The use of chemical tracers, temperature, groundwater ages (this study), and numerical modeling provide evidence for cross-fault flow (Moeck et al., 2016, 2017a, 2018a, 2020; Popp et al., 2019). Furthermore, observation well C.206 has a distinct geochemical signature and age, which could not be classed with any other investigated well. This is in line with the results from a multicomponent statistical analysis where well C.206 was identified with a distinctly different Ca^{2+}-CO_2 pressure relationship compared to all other wells, and was, therefore, treated as an exception (Moeck et al., 2016). Based on the Bayesian mixing model (Popp et al., 2019), paired with apparent age estimates, we can now explain these different characteristics by the presence of a high ratio (36%) of a previously unknown water source (Flexure zone with fractures) associated with an older groundwater age (36.6 years) and a higher PCE concentration. This sampling point situated in the vicinity of the Rhine Valley Flexure zone suggests that faults can play a role as preferential flow paths for the transport of old groundwater, which is richer in helium and has an elevated PCE concentration.

6. Summary and conclusions

In urban areas, groundwater management is often challenged by contamination. Management, therefore, requires a thorough and robust scientific understanding of flow and transport processes, as well as groundwater residence time. Environmental tracers, such as tritium and the decay product helium, have been shown to efficiently determine the source of groundwater, in order to gain insight into flow and transport processes, and to determine groundwater residence times. However, the analysis is expensive and labor- and time-intensive, therefore, potentially limiting the amount of possible sampling locations.

In contrast, new developments in a portable field-operated GE-MIMS system provides a unique opportunity to measure dissolved gas concentrations, such as ^{4}He, relatively quickly and inexpensively. Due to technical and analytical differences between the two methods, laboratory- ^{3}H/^{3}He age and field-based GE-MIMS ^{4}He analysis yielding comparable results is not straightforward.

We establish an inter-relationship between ^{3}H/^{3}He apparent groundwater age and ^{4}He measured with the GE-MIMS, and demonstrate that the results of the simpler GE-MIMS system are as satisfactory as those of the highly sophisticated lab-based method. Thus, the combined use of laboratory and predicted groundwater ages (based on the GE-MIMS relationship) opens up new opportunities in site characterization, even though laboratory data are still required to establish this relationship for each study site. The applicability of the method is assured when radiogenic helium is accumulated in the aquifer by radioactive decay of U and Th within the aquifer matrix; therefore, the ^{4}He concentration is controlled by the residence time of the groundwater in the aquifer. The demonstrated analysis reveals valuable insights into the conceptual understanding of groundwater systems. The analysis has the potential to provide crucial information regarding the dynamics of groundwater systems (residence time, mixing, flow regime, etc.), and can be useful for a large range of hydrogeological projects (aquifer vulnerability, contaminated sites, groundwater resource assessments, sustainability studies, geothermal assessments, quantification of groundwater mixing, calibration/verification of numerical models, etc.). Additionally, the GE-MIMS is able to measure various gases, and might provide further opportunities to investigate a study site from further perspectives.

For our study site, we combined the laboratory-based and predicted apparent ages with hydrochemical data, water isotopes, and PCE concentrations to identify spatial inter-aquifer mixing in the subsurface. This approach allowed us to identify the spatial pattern of mixing between recent artificially infiltrated groundwater and water originating from the regional flow path. We found a strong correlation between groundwater ages and PCE concentrations. Overall, low PCE concentrations and young groundwater ages occur when the fraction of artificially infiltrated water is high. Moreover, for some wells, fault-induced aquifer connectivity is recognized, suggesting that the faults play a major role as preferential flow paths for the transport of old groundwater richer in helium and elevated PCE concentrations.

Declaration of competing interest

None.

Acknowledgments

The authors acknowledge the financial support from the canton of Basel-Landschaft, Switzerland in the framework of the project “Regionale Wasserversorgung Basel-Landschaft 21”. C.M. acknowledges financial support from the Swiss National Science Foundation (grant no. IZK0Z2_173680). A.L.P. acknowledges financial support from the EU Framework Programme for Research and Innovation Horizon 2020 ITNs “Hypotrain” (grant no. 641939). Additionally, the authors thank the two anonymous reviewers for their valuable and constructive feedback that helped to improve the original manuscript.

References

Aeschbach-Hertig, W., et al., 1998. A 3H/3He study of ground water flow in a fractured bedrock aquifer. Groundwater 36 (4), 661–670.
Aeschbach-Hertig, W., Peeters, F., Beyerle, U., Kipfer, R., 2000. Palaeotemperature reconstruction from noble gases in ground water taking into account equilibration with entrapped air. Nature 405 (6790), 1040–1044.
Auckenthaler, A., Bänninger, D., Affolter, A., Zechner, E., Huggenberger, P., 2010. Drinking water production close to contaminant sites: a case study from the region of Basel, Switzerland. In: Proceedings of the 7th International Groundwater Quality Conference GQ, pp. 167–170.
Baillieux, A., Moeck, C., Perrochet, P., Hunkeler, D., 2015. Assessing groundwater quality trends in pumping wells using spatially varying transfer functions. Hydrogeol. J. 23 (7), 1449–1463.
Battle-Aguilar, J., et al., 2017. Groundwater residence time and aquifer recharge in multilayered, semi-confined and faulted aquifer systems using environmental tracers. J. Hydrol. 546, 150–165.
Bertrand, G., et al., 2016. Groundwater contamination in coastal urban areas: anthropogenic pressure and natural attenuation processes. Example of Recife (PE State, NE Brazil). J. Contam. Hydrol. 192, 165–180.
Beyerle, U., et al., 1999. Infiltration of river water to a shallow aquifer investigated with ^{3}H/^{3}He, noble gases and CFCs. J. Hydrol. 220 (3), 169–185.

Beyerle, U., et al., 2000. A mass spectrometric system for the analysis of noble gases and tritium from water samples. Environ. Sci. Technol. 34 (10), 2042–2050.

Brennwald, M.S., Schmidt, M., Oser, J., Kipfer, R., 2016. A portable and autonomous mass spectrometric system for on-site environmental gas analysis. Environ. Sci. Technol. 50 (24), 13455–13463.

Brennwald, M.S., Tomonaga, Y., Kipfer, R., 2020. Deconvolution and compensation of mass spectrometric overlap interferences with the miniRUEDI portable mass spectrometer. MethodsX 7, 1–11, 101038.

Burri, N.M., Weatherl, R., Moeck, C., Schirmer, M., 2019. A review of threats to groundwater quality in the anthropocene. Sci. Total Environ. 684, 136–154.

Chambers, L.A., Gooddy, D.C., Binley, A.M., 2019. Use and application of CFC-11, CFC-12, CFC-113 and SF_6 as environmental tracers of groundwater residence time: a review. Geosci. Front. 10 (5), 1643–1652.

Cirpka, O.A., Kitanidis, P.K., 2000. Characterization of mixing and dilution in heterogeneous aquifers by means of local temporal moments. Water Resour. Res. 36 (5), 1221–1236.

Cook, P.G., Böhlke, J.-K., 2000. Determining timescales for groundwater flow and solute transport. In: Cook, P.G., Herczeg, A.L. (Eds.), Environmental Tracers in Subsurface Hydrology. Springer US, Boston, pp. 1–30.

Cook, P.G., Herczeg, A.L. (Eds.), 2012. Environmental Tracers in Subsurface Hydrology. Springer Science & Business Media.

Cook, P.G., Solomon, D.K., 1995. Transport of atmospheric trace gases to the water table: implications for groundwater dating with chlorofluorocarbons and krypton 85. Water Resour. Res. 31 (2), 263–270.

Cook, P.G., Solomon, D.K., 1997. Recent advances in dating young groundwater: chlorofluorocarbons, $^3H/^3He$ and ^{85}Kr. J. Hydrol. 191 (1), 245–265.

Corcho Alvarado, J.A., et al., 2005. ^{36}Cl in modern groundwater dated by a multi-tracer approach ($^3H/^3He$, SF_6, CFC-12 and ^{85}Kr): a case study in quaternary sand aquifers in the Odense Pilot River Basin, Denmark. Appl. Geochem. 20 (3), 599–609.

Corcho Alvarado, J.A., et al., 2007. Constraining the age distribution of highly mixed groundwater using ^{39}Ar: a multiple environmental tracer ($^3H/^3He$, ^{85}Kr, ^{39}Ar, and ^{14}C) study in the semiconfined Fontainebleau Sands Aquifer (France). Water Resour. Res. 43 (3).

de Graaf, I.E.M., van Beek, L.P.H., Wada, Y., Bierkens, M.F.P., 2014. Dynamic attribution of global water demand to surface water and groundwater resources: effects of abstractions and return flows on river discharges. Adv. Water Resour. 64, 21–33.

Ekwurzel, B., et al., 1994. Dating of shallow groundwater: comparison of the transient tracers $^3H/^3He$, chlorofluorocarbons, and ^{85}Kr. Water Resour. Res. 30 (6), 1693–1708.

Fienen, M., Hunt, R., Krabbenhoft, D., Clemo, T., 2009. Obtaining parsimonious hydraulic conductivity fields using head and transport observations: a Bayesian geostatistical parameter estimation approach. Water Resour. Res. 45 (8).

Gleeson, T., et al., 2012. Towards sustainable groundwater use: setting long-term goals, backcasting, and managing adaptively. Groundwater 50 (1), 19–26.

Gooddy, D.C., Darling, W.G., Abesser, C., Lapworth, D.J., 2006. Using chlorofluorocarbons (CFCs) and sulphur hexafluoride (SF_6) to characterise groundwater movement and residence time in a lowland Chalk catchment. J. Hydrol. 330 (1–2), 44–52.

Güler, C., Thyne, G.D., McCray, J.E., Turner, A.K., 2002. Evaluation of graphical and multivariate statistical methods for classification of water chemistry data. Hydrogeol. J. 10 (4), 455–474.

Jasechko, S., 2016. Partitioning young and old groundwater with geochemical tracers. Chem. Geol. 427, 35–42.

Karges, U., Becker, J., Püttmann, W., 2018. 1,4-Dioxane pollution at contaminated groundwater sites in western Germany and its distribution within a TCE plume. Sci. Total Environ. 619–620, 712–720.

Kipfer, R., Aeschbach-Hertig, W., Peeters, F., Stute, M., 2002. Noble gases in lakes and ground waters. Rev. Mineral. Geochem. 47 (1), 615–700.

Kitanidis, P.K., 2015. Persistent questions of heterogeneity, uncertainty, and scale in subsurface flow and transport. Water Resour. Res. 51 (8), 5888–5904.

Knapp, J.L., Osenbrück, K., Brennwald, M.S., Cirpka, O.A., 2019. In-situ mass spectrometry improves the estimation of stream reaeration from gas-tracer tests. Sci. Total Environ. 655, 1062–1070.

Koltermann, C.E., Gorelick, S.M., 1996. Heterogeneity in sedimentary deposits: a review of structure-imitating, process-imitating, and descriptive approaches. Water Resour. Res. 32 (9), 2617–2658.

LaBolle, E.M., Fogg, G.E., Eweis, J.B., 2006. Diffusive fractionation of ^3H and ^3He in groundwater and its impact on groundwater age estimates. Water Resour. Res. 42 (7).

Lehmann, B.E., et al., 2003. A comparison of groundwater dating with ^{81}Kr, ^{36}Cl and ^4He in four wells of the Great Artesian Basin, Australia. Earth Planet. Sci. Lett. 211 (3), 237–250.

Levison, J., Novakowski, K., Reiner, E.J., Kolic, T., 2012. Potential of groundwater contamination by polybrominated diphenyl ethers (PBDEs) in a sensitive bedrock aquifer (Canada). Hydrogeol. J. 20 (2), 401–412.

Mächler, L., Brennwald, M.S., Kipfer, R., 2012. Membrane inlet mass spectrometer for the quasi-continuous on-site analysis of dissolved gases in groundwater. Environ. Sci. Technol. 46 (15), 8288–8296.

Mächler, L., Peter, S., Brennwald, M.S., Kipfer, R., 2013. Excess air formation as a mechanism for delivering oxygen to groundwater. Water Resour. Res. 49 (10), 6847–6856.

Mächler, L., Brennwald, M.S., Tyroller, L., Livingstone, D.M., Kipfer, R., 2014. Conquering the outdoors with on-site mass spectrometry. CHIMIA Int. J. Chem. 68 (3), 155–159.

Mackay, D.M., Roberts, P.V., Cherry, J.A., 1985. Transport of organic contaminants in groundwater. Environ. Sci. Technol. 19 (5), 384–392.

Manning, A.H., Caine, J.S., 2007. Groundwater noble gas, age, and temperature signatures in an Alpine watershed: valuable tools in conceptual model development. Water Resour. Res. 43 (4).

Manning, A.H., Solomon, D.K., Thiros, S.A., 2005. $^3H/^3He$ age data in assessing the susceptibility of wells to contamination. Groundwater 43 (3), 353–367.

Massmann, G., Sültenfuß, J., Pekdeger, A., 2009. Analysis of long-term dispersion in a river-recharged aquifer using tritium/helium data. Water Resour. Res. 45 (2).

McCallum, J.L., Engdahl, N.B., Ginn, T.R., Cook, P.G., 2014. Nonparametric estimation of groundwater residence time distributions: what can environmental tracer data tell us about groundwater residence time? Water Resour. Res. 50 (3), 2022–2038.

Minnig, M., Moeck, C., Radny, D., Schirmer, M., 2018. Impact of urbanization on groundwater recharge rates in Dübendorf, Switzerland. J. Hydrol. 563, 1135–1146.

Moeck, C., et al., 2016. Multicomponent statistical analysis to identify flow and transport processes in a highly-complex environment. J. Hydrol. 542, 437–449.

Moeck, C., et al., 2017a. Estimating the spatial distribution of artificial groundwater recharge using multiple tracers. Isot. Environ. Health Stud. 53 (5), 484–499.

Moeck, C., et al., 2017b. Characterization of a managed aquifer recharge system using multiple tracers. Sci. Total Environ. 609, 701–714.

Moeck, C., et al., 2018a. Improved water resource management for a highly complex environment using three-dimensional groundwater modelling. Hydrogeol. J. 26 (1), 133–146.

Moeck, C., et al., 2018b. Verteilung anthropogen eingetragener Stoffe im Grundwasser: Ein Fallbeispiel aus der Nordschweiz [Spatial distribution of anthropogenic inputs into groundwater: a case study]. Grundwasser 23 (4), 297–309.

Moeck, C., Molson, J., Schirmer, M., 2020. Pathline density distributions in a null-space Monte Carlo approach to assess groundwater pathways. Groundwater 58 (2), 189–207.

Navarro, A., Carbonell, M., 2007. Evaluation of groundwater contamination beneath an urban environment: the Besòs river basin (Barcelona, Spain). J. Environ. Manag. 85 (2), 259–269.

Palau, J., et al., 2014. Multi-isotope (carbon and chlorine) analysis for fingerprinting and site characterization at a fractured bedrock aquifer contaminated by chlorinated ethenes. Sci. Total Environ. 475, 61–70.

Peeters, F., et al., 2003. Improving noble gas based paleoclimate reconstruction and groundwater dating using $^{20}Ne/^{22}Ne$ ratios. Geochim. Cosmochim. Acta 67 (4), 587–600.

Perrin, J., Parker, B.L., Cherry, J.A., 2011. Assessing the flow regime in a contaminated fractured and karstic dolostone aquifer supplying municipal water. J. Hydrol. 400 (3–4), 396–410.

Poeter, E., Gaylord, D.R., 1990. Influence of aquifer heterogeneity on contaminant transport at the Hanford site. Groundwater 28 (6), 900–909.

Popp, A.L., Scheidegger, A., Moeck, C., Brennwald, M.S., Kipfer, R., 2019. Integrating Bayesian groundwater mixing modeling with on-site helium analysis to identify unknown water sources. Water Resour. Res. 55 (12), 10602–10615.

Popp, A.L., Manning, C.C., Brennwald, M.S., Kipfer, R., 2020. A new in situ method for tracing denitrification in riparian groundwater. Environ. Sci. Technol. 54 (3), 1562–1572.

Regli, C., Rauber, M., Huggenberger, P., 2003. Analysis of aquifer heterogeneity within a well capture zone, comparison of model data with field experiments: a case study from the river Wiese, Switzerland. Aquat. Sci. 65 (2), 111–128.

Renard, P., 2007. Stochastic hydrogeology: what professionals really need? Groundwater 45 (5), 531–541.

Roques, C., et al., 2020. In situ observation of helium and argon release during fluid-pressure-triggered rock deformation. Sci. Rep. 10 (1), 6949.

Sanford, W.E., 2011. Calibration of models using groundwater age. Hydrogeol. J. 19 (1), 13–16.

Schilling, O.S., Cook, P.G., Brunner, P., 2019. Beyond classical observations in hydrogeology: the advantages of including exchange flux, temperature, tracer concentration, residence time, and soil moisture observations in groundwater model calibration. Rev. Geophys. 57 (1), 146–182.

Schirmer, M., Leschik, S., Musolff, A., 2013. Current research in urban hydrogeology – a review. Adv. Water Resour. 51, 280–291.

Schlosser, P., Stute, M., Sonntag, C., Münnich, K.O., 1989. Tritiogenic ^3He in shallow groundwater. Earth Planet. Sci. Lett. 94 (3–4), 245–256.

Slough, K.J., Sudicky, E.A., Forsyth, P.A., 1999. Numerical simulation of multiphase flow and phase partitioning in discretely fractured geologic media. J. Contam. Hydrol. 40 (2), 107–136.

Solomon, D.K., 2000. 4He in groundwater. In: Cook, P.G., Herczeg, A.L. (Eds.), Environmental Tracers in Subsurface Hydrology. Springer US, Boston, pp. 425–439.

Solomon, D.K., Poreda, R.J., Schiff, S.L., Cherry, J.A., 1992. Tritium and helium: 3 as groundwater age tracers in the Borden aquifer. Water Resour. Res. 28 (3), 741–755.

Solomon, D.K., Schiff, S.L., Poreda, R.J., Clarke, W.B., 1993. A validation of the $^3H/^3He$ method for determining groundwater recharge. Water Resour. Res. 29 (9), 2951–2962.

Spottke, I., Zechner, E., Huggenberger, P., 2005. The southeastern border of the Upper Rhine Graben: a 3D geological model and its importance for tectonics and groundwater flow. Int. J. Earth Sci. 94 (4), 580–593.

Suckow, A., 2014. The age of groundwater – definitions, models and why we do not need this term. Appl. Geochem. 50, 222–230.

Szabo, Z., et al., 1996. Age dating of shallow groundwater with chlorofluorocarbons, tritium/helium: 3, and flow path analysis, Southern New Jersey Coastal Plain. Water Resour. Res. 32 (4), 1023–1038.

Therrien, R., Sudicky, E.A., 1996. Three-dimensional analysis of variably-saturated flow and solute transport in discretely-fractured porous media. J. Contam. Hydrol. 23 (1–2), 1–44.

Tolstikhin, I., Kamenskiy, I.L., 1969. Determination of groundwater age by the T-^{3}He method. Geochem. Int. 6, 810–811.
Tomonaga, Y., et al., 2019. On-line monitoring of the gas composition in the Full-scale Emplacement experiment at Mont Terri (Switzerland). Appl. Geochem. 100, 234–243.
Torgersen, T., Clarke, W.B., 1985. Helium accumulation in groundwater, I: an evaluation of sources and the continental flux of crustal ^{4}He in the Great Artesian Basin, Australia. Geochim. Cosmochim. Acta 49 (5), 1211–1218.
Vázquez-Suñé, E., Sánchez-Vila, X., Carrera, J., 2005. Introductory review of specific factors influencing urban groundwater, an emerging branch of hydrogeology, with reference to Barcelona, Spain. Hydrogeol. J. 13 (3), 522–533.
Visser, A., Broers, H.P., Purtschert, R., Sültenfuß, J., de Jonge, M., 2013. Groundwater age distributions at a public drinking water supply well field derived from multiple age tracers (^{85}Kr, ^{3}H/^{3}He, and ^{39}Ar). Water Resour. Res. 49 (11), 7778–7796.
Weber, U.W., Cook, P.G., Brennwald, M.S., Kipfer, R., Stieglitz, T.C., 2018. A novel approach to quantify air–water gas exchange in shallow surface waters using high-resolution time series of dissolved atmospheric gases. Environ. Sci. Technol. 53 (3), 1463–1470.
Wei, W., Aeschbach-Hertig, W., Chen, Z.Y., 2015. Identification of He sources and estimation of He ages in groundwater of the North China Plain. Appl. Geochem. 63, 182–189.